Records of Ground Deformation in Northern Kefalonia by Cosmogenic ^{36}Cl Geochronology

Constantin D. Athanassas *, Regis Braucher, Ioannis Vakalas, George Apostolopoulos

Posted Date: 6 January 2025

doi: 10.20944/preprints202501.0414.v1

Keywords: exposure dating; landslide; anticline; rupture; slope stability

Article

Records of Ground Deformation in Northern Kefalonia by Cosmogenic ^{36}Cl Geochronology

Constantin D. Athanassas [1,*], Regis Braucher [2], Ioannis Vakalas [1] and George Apostolopoulos [1]

[1] School of Mining and Metallurgical Engineering, National Technical University of Athens (NTUA), 15780, Greece

[2] CEREGE, Aix Marseille Université, CNRS, IRD, INRAE, Collège de France, Aix-en-Provence, cedex 04, France

* Correspondence: constathanassas@metal.ntua.gr

Abstract: The cosmogenic ^{36}Cl exposure ages in this study provide the first direct chronology of landscape evolution and ground deformation in the Ionian Islands, with a focus on the Thinia Valley and the anticline near Zola in northern Kefalonia, western Greece. At the primary Zola site, cosmogenic ^{36}Cl exposure ages indicate persistent deformation on the eastern limb of the anticline from the Middle Quaternary to historical times. This broad age range suggests that the anticline has experienced multiple deformation events rather than a single episode. Older ages correspond to a Middle Pleistocene phase of exhumation, while younger ages suggest additional mass-wasting events influenced by climatic and tectonic factors. At the secondary site, Kourouklata, southeast of the previous site, ages indicate a steady-state surface where erosion and decay balance cosmogenic ^{36}Cl production, implying a true age beyond the dating range and leaving the slope's origin indeterminate. Nonetheless, recent tectonic activity on a fault cutting through this surface suggests an actively evolving tectonic landscape continuing into the Holocene.

Keywords: exposure dating; landslide; anticline; rupture; slope stability

1. Introduction

Off the Ionian coasts of Greece, the active boundary of the Hellenic Arc involves the subduction of the oceanic lithosphere of the Eastern Mediterranean under both the con-tinental Apulian (or Adriatic) and Aegean microplates as well as the continental collision of the Adriatic microplate onto Eurasia [1–6]. Around Kefalonia (Figure 1), conver-gence is expressed by the Kefalonia Transform Fault (KFT) which accommodates dextral strike-slip motion [5,7]. The KTF exhibits the highest crustal deformation rates in the Aegean area (s.l.), with slip rates up to 25–30 mm·yr^{-1} [8–12]. Therefore, Kefalonia falls into a seismically active, broad and right-lateral strike-slip crustal shear zone [3,5,12–15]. Additionally, slip rates of 14.3 mm·yr^{-1} occur in the southern Paliki Peninsula (Figure 1). These high deformation rates result in frequent earthquakes with Mw > 6.0 [16] with a cyclicity ranging from 34 to nearly 300 years [12]. This temporal pattern is explained by stress transfer among adjacent fault segments [12,15]. Seismic activity has been ongoing, with the August 1953 seismic sequence of KFT (Mw = 6.8) being the most destructive event in the recent history of Greece ([16–24] and references therein).

Onshore Kefalonia, compressional tectonics dominates. A major thrust fault, the Ionian Thrust (Figure 1) marks the outermost Hellenide (Alpine) nappe, the Ionian nappe. The nappe exhibits notable northwest-southeast trending folds and thrust faults [25,26] within the Lower Jurassic carbonates of the Ionian zone and is emplaced onto the rela-tively stable Apulian autochthon of the Paxoi (or Pre-Apulian) unit on the eastern pe-riphery of the Apulian plate [3]. While the precise age of all thrusts in the external regions of the Ionian nappe may not always be determined, they are evidently post-Miocene [3]. Several hrust faults have been identified as Plio-Quaternary in age as

 doi:10.20944/preprints202501.0414.v1

Mesozoic carbonates overthrust not only Miocene but Pliocene and Quaternary strata [3,26]. These are partially explained by the ongoing westward Hellenide deformation [3] and partially by the rollback of the Hellenic slab [3,6,27–31] and references therein, [32,33].

Tectonic strain has been steadily accumulating on the topography of Kefalonia as documented by [17,18,21,23]. Reverse faulting and subsequent folding are responsible for the generation of important relief in mountain ranges. Hermanns et al. [33,34] and Strecker and Marrett [35] showed that the frequency and location of landslides shifts in tandem with the motion of reverse faults. Slope failure then begins to operate [34–39]. Most topographic relief on Kefalonia associated with thrust faults is located in the uplifting hanging walls, creating sharply dipping topographic slopes. In northern Kefalonia, a pair of such extensive hanging walls are drawing near to each other forming a NNE-SSW trending isthmus, stretching between the Gulf of Argostoli and the Ionian Sea, known as the Thinia Valley (Figure 1). The Thinia Valley is bordered to the east by the western flanks of Mount Aenos (Figures 1 and 2).

In tectonic regimes such as Kefalonia, several hundreds of smaller seismic events may occur each year (with major ones every few decades or centuries). Consequently, the stability of the bedrock becomes crucial, and in the event of a subsequent tectonic pulse, the structure becomes susceptible to gravitational collapse. North Kefalonia has experi-enced such co-seismic slope failure, observable in both contemporary times [24] and in the past [40,41]. The hillslopes of the Thinia valley are notably unstable, often experiencing periodic landslips due to failures along bedding planes [24,40,41] and that has led to the valley becoming infilled [40,41]. Consequently, the present valley configuration appears to be controlled not only by the bedrock geology and tectonics but also by recent processes of mass-wasting that led to its becoming infilled [40,41].

Numerical dating is crucial for characterizing the nature and the frequency of slope failure on Kefalonia. Cosmogenic ^{36}Cl accumulated on bedrock surfaces has been found to be most suitable for dating landforms shaped on carbonate rocks [43–46]. Spe-cifically, cosmogenic nuclides produced in bedrock surfaces in situ (also known as ter-restrial cosmogenic nuclides – TCN) are the technique of choice for numerical dating of fault escarpments [43–52] and references in these articles). As of now, there have been relatively few attempts to exposure-date ancient landslides (e.g., [52–61,70]). Therefore, exposure dating of landforms across the Thinia valley associated with slope failure using cosmogenic 36Cl holds a mo-tivating challenge and opens up the possibility of exploring the frequency and origin of ground deformation in northern Kefalonia.

2. Geological Setting and Samples

Kefalonia, in common with the rest of the southern Ionian Islands (Ithaca and Zakynthos), mainly consists (Figure 1) of the alpine geotectonic units of the Paxoi (also known as Pre-Apulian as it represents the transition to the Apulian platform [3]) and the Ionian unit. The latter is the lithological content of the Ionian nappe (Figure 1). The Upper Triassic - Upper Cretaceous carbonate sequence of the Ionian unit (relatively allochthonous) is thrust on the Cretaceous carbonates and the Middle Miocene–Early Pliocene clastic sequence (consisting of marls, clays and limestones) of the Paxoi unit (relatively autochthonous via the subhorizontal Ionian thrust [3]. The Ionian nappe is emplaced through the thrust onto Miocene rocks of the Paxoi unit [3,26]. Post-alpine deposits of Pliocene - Quaternary age lying unconformably on the alpine basement [3,26].

 doi:10.20944/preprints202501.0414.v1

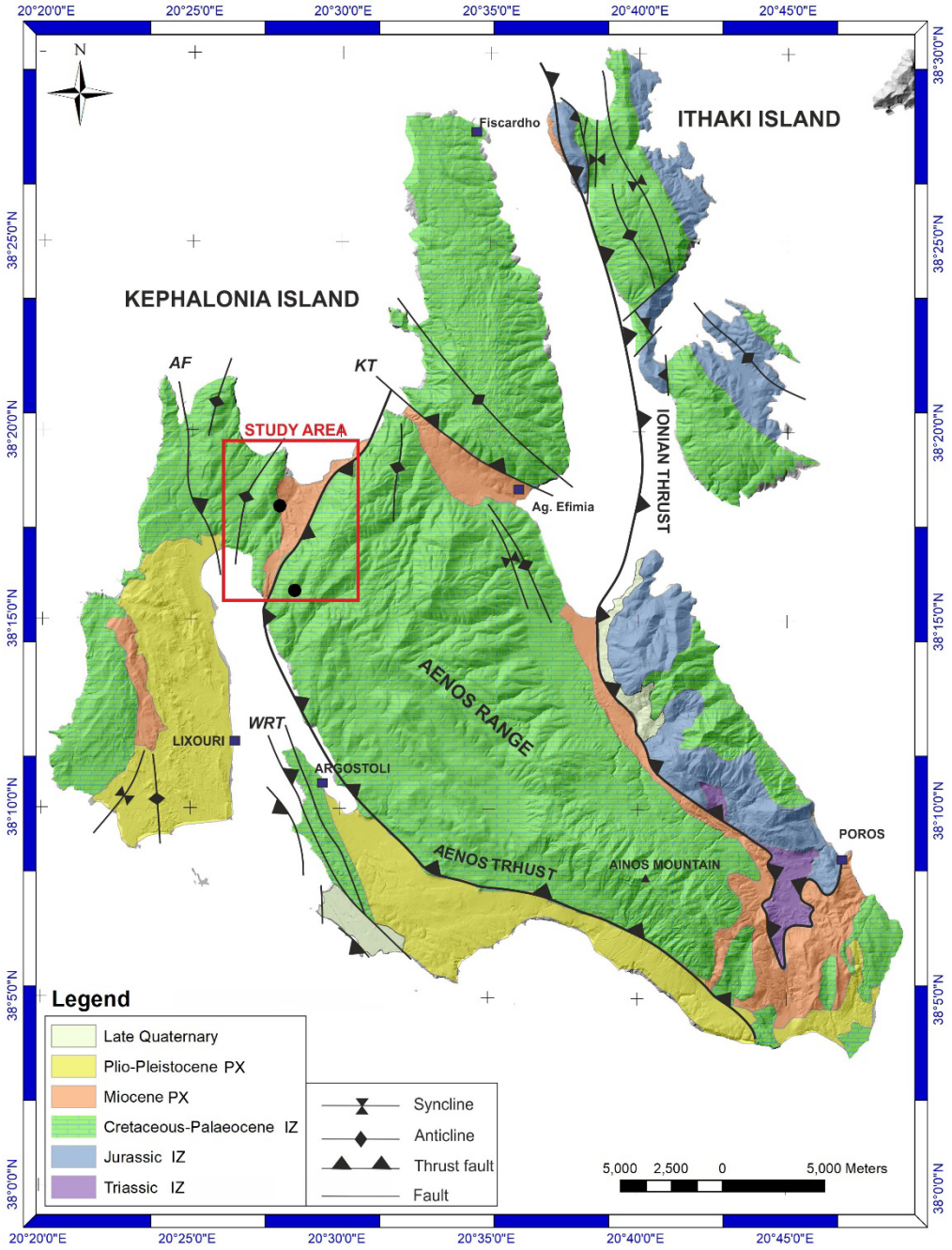

Figure 1. Geological map of Kefalonia compiled with information from the Geological Map of Greece (Sheet: Island of Kefalonia Northern and Southern Section, scale 1:50,000, Institute of Geological and Mineral Research - IGME) as well as from [25] and [3]. The red square encloses the Thinia Valley and the study area and the bold dots within it the study sites.

Compressional tectonics dominates the structure of the Ionian zone on Kefalonia. Shortening is evident throughout the island [3] as the available geological studies reveal [3,25]. A series of approximately north-south trending folds and at least one major thrust fault can be traced: the Aenos Thrust (Figure 1) is a major geological boundary that places the Mesozoic carbonates on the Miocene marls, marked by a prominent scarp (Figures 2 and 3).

 doi:10.20944/preprints202501.0414.v1

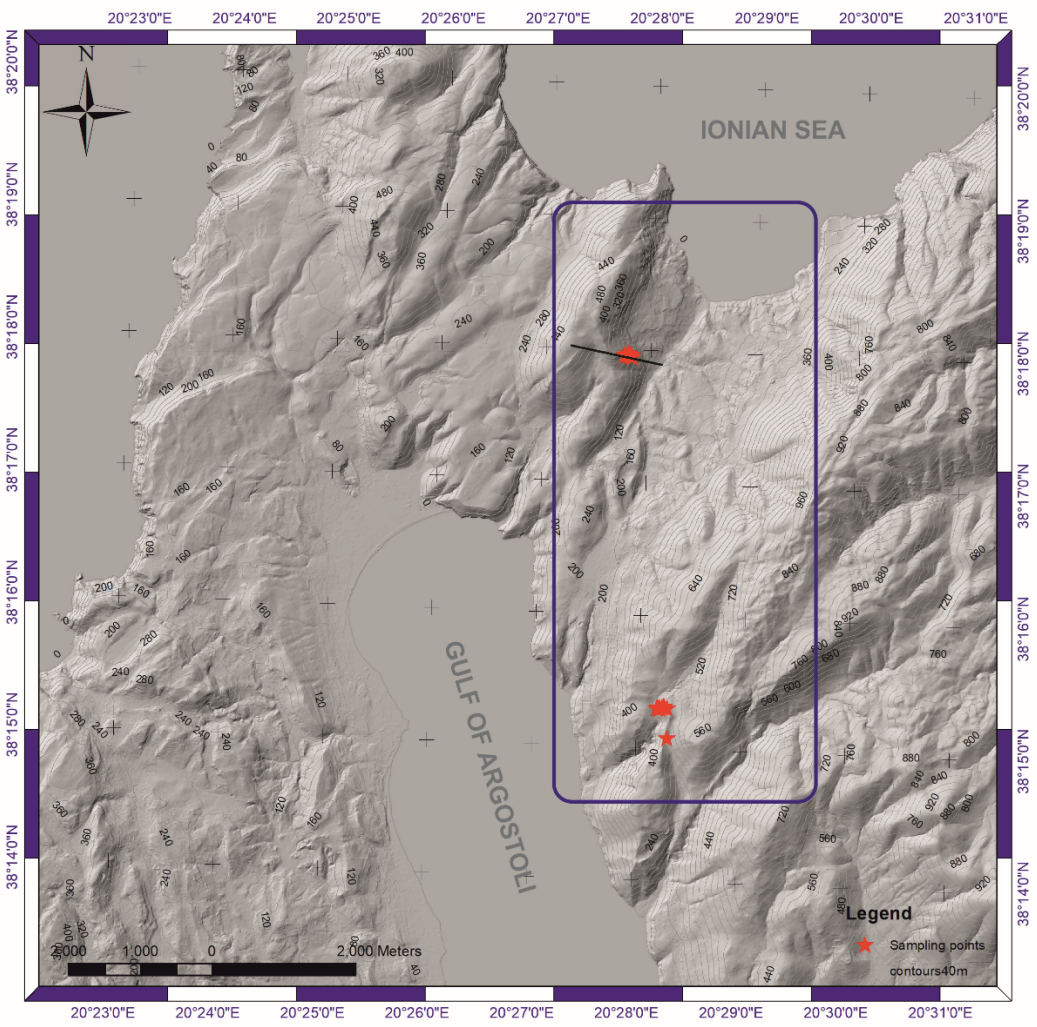

Figure 2. Relief (topographic aspect) map of northern Kefalonia and the study area. The blue rectangular marks the NE-SW trending Thinia Valley, stretching between the Gulf of Argostoli and the Ionian Sea, while the two clusters of red points mark the sample/study locations. The prominent mountainsides along the eastern boundary of the valley represent the morphological expression of the Aenos Thrust. (source: Helelnic Cadastre). Black line across the sample spots corresponds to the direction of the geological cross-section shown in Figure 3.

The Thinia Valley lies between the Gulf of Argostoli to the south and the Ionian Sea to the north (Figure 2). It spans a distance of 6 km with a maximum width of 2 km and an elevation at its center of approximately 180 m.a.s.l. Enclosed by steep hill ranges on both sides, the eastern flank reaches heights of nearly 1 km. The Paxoi carbonate rocks are overlain unconformably by Miocene marls (Figures 1 and 3) and clastic sediments which on the west slopes of the valley they dip gently eastward too (Figure 3). The easterly dip increases towards the north and reach their highest values near Zola (Figure 4).

According to field studies [40,41] around Zola, folding is expressed by two distinct bedding dips of the Cretaceous and Paleogene limestones, ~30° WNW and ~60° ENE respectively implying an asymmetric, inclined, east-verging anticline structure. The anticline hinge is tentatively delineated in Figure 4. There is a significant dichotomy in the amount of ground deformation between the eastern and western limbs of the anticline (Figure 5). The western slopes exhibit nearly homogenous slope in the NW direction with no visible signs of failure (Figure 5a). In contrast, the ground on the eastern slopes of the anticline (western walls of the Thinia Valley) appear greately deformed, with the Zola landslide being the most prominent natural terrain feature. The Zola landslide is well-defined by a ~300 m deep head scarp encircled by a ~ 3 km long crown in the perimeter. The landslide could be classified [42] as a rotational sliding with local translational sliding (block slide). The ENE dips

 doi:10.20944/preprints202501.0414.v1

constrain the strata on the east limb of the structure to descend into the valley and this sets things up for failure. The toe of the landslide may be controlled by a thrust that has been deformed into a normal structure by long-term creep [40,41].

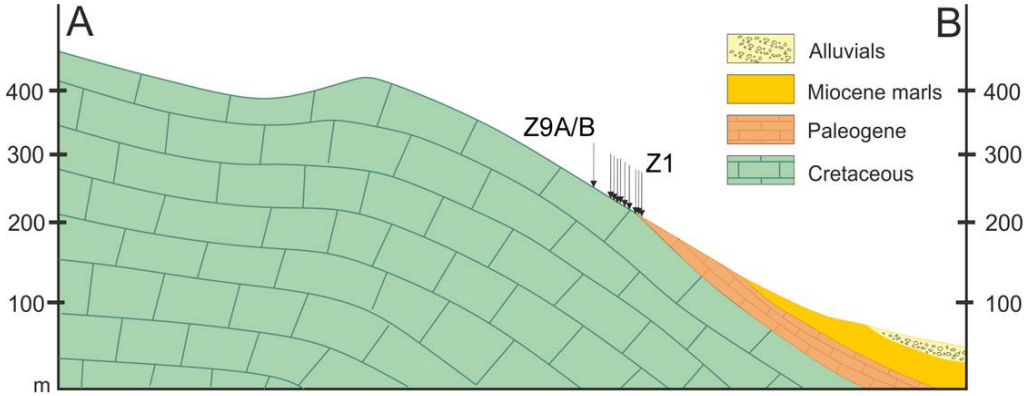

Figure 3. Generalized geological cross-section (compiled from field data and from [40] Figure 10 therein) of the western part of the Thinia Valley which features Cretaceous and Paleogene limestones overlain by Miocene sediments, both dipping gently eastward. Sample positions are indicated also. The length corresponds to the linear segment AB in Figure 5a.

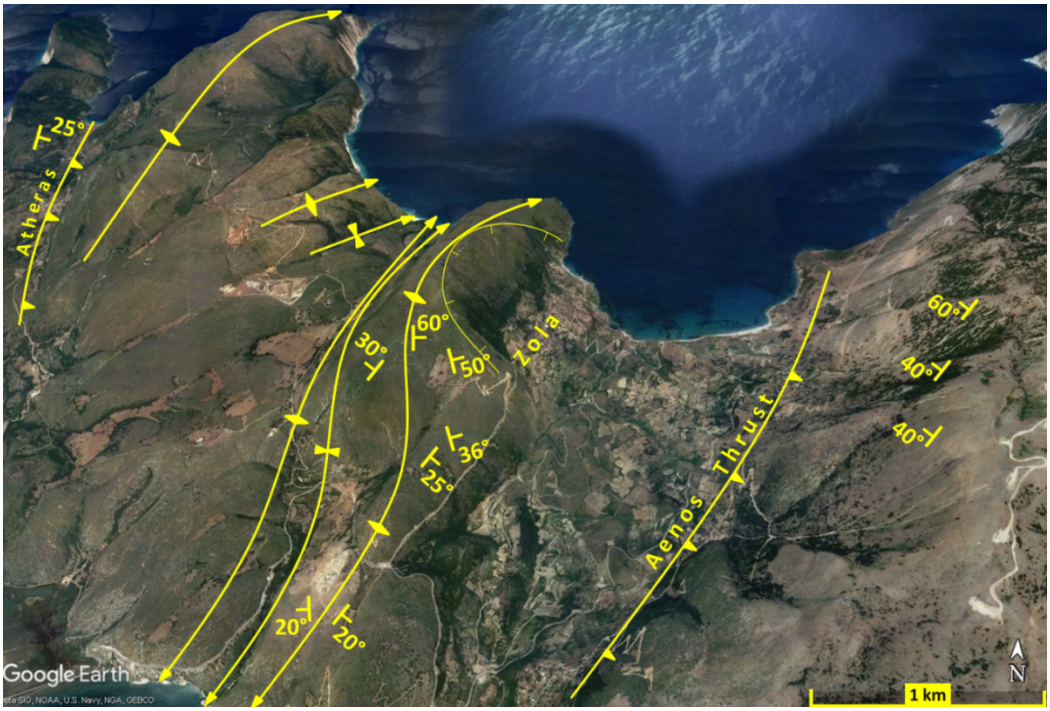

Figure 4. Illustration of tectonic context (according to [3]) around the Zola landslide, at the NW end of the Thinia Valley. Ticks perpendicular to the line marking the crown of the concave break of the slope. View to the North. North arrow on left-down. Basemap: Google Earth.

 doi:10.20944/preprints202501.0414.v1

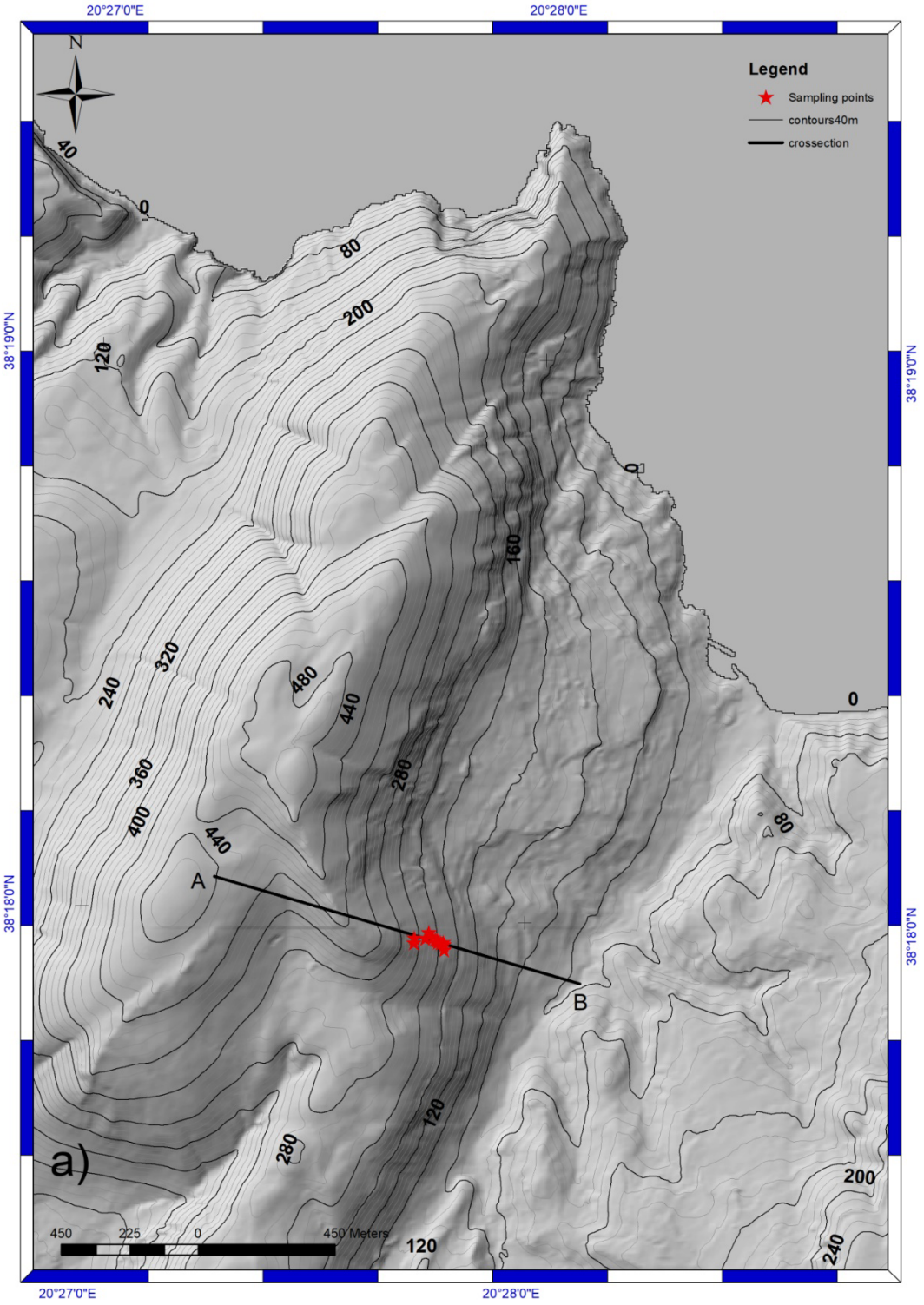

 doi:10.20944/preprints202501.0414.v1

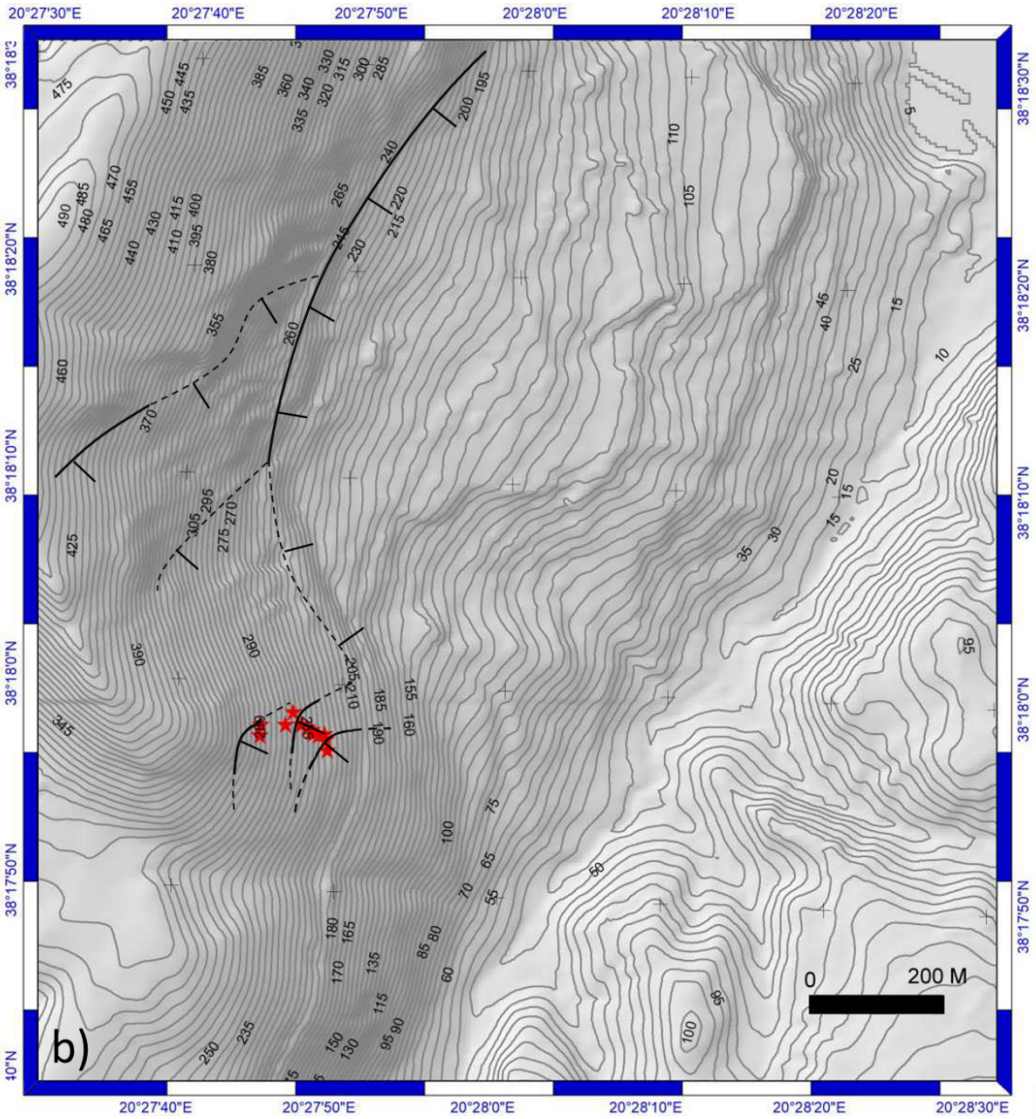

Figure 5. a) Topography of the NE-SW trending anticline ridge that bounds the Thinia Valley to the east. Ground deformation on the eastern slopes of the anticline ridge is more frequent than on the western slopes. The contours (20 - m spacing) of the hinge deflect to the NW, possibly implying a deflected antincline axis as well. This is a common feature in fold-thrust belts, where the hinge line may curve due to strike/oblique-slip faults altering the geometry of the fold. b) Close-up of the rectangular area shown above, largely corresponding to the Zola landslide. Contours (10-m spacing) are overlaid on a digital terrain model. Deformation features (traced using blink comparison of historical imagery on Google Earth) are shown with solid lines (while their probable extension is shown with dashed lines). Ticks point to the direction of subsidence. The topographic map of the Zola area shows red stars representing sample locations. DEM sourced from the Hellenic Cadastre.

A close-up of the digital terrain model (Figure 5b) reveals several topographic breaks that are difficult to identify from ground level. Blink comparison of Google Earth imagery highlights these terrain features through temporal changes in reflectance and color. Notably, the 2013 imagery revealed several ruptures on the eastern limb, indicating normal sense of motion (Figure 5b), with likely many more ruptures (both rotational and translational) either obscured by vegetation or detectable with higher resolution imagery. In essence, folding induces slope collapse and sliding, rendering the western slopes of the Thinia Valley a polygenetic terrain, shaped by the blending of various endogenetic and exogenic processes.

Figure 6 offers a more comprehensive perspective of the Zola landslide (viewed in a SW direction) and of the sample sites. The eastern slopes of the valley (Figure 4) constitute the western limb of a significant hanging-wall anticline, a direct outcome of the Aenos Thrust emplacement. The

 doi:10.20944/preprints202501.0414.v1

Aenos Thrust has displaced the westward-dipping Cretaceous-Paleocene limestones onto the eastward-dipping Miocene sediments although the precise location of the thrust is often obscured by rockfall debris [3,23,40,41]. The steep westerly dips of the Cretaceous and Paleogene limestones range from 45° to greater than 60°. The valley walls have experienced periodic landslips from both mountansides [40,41].

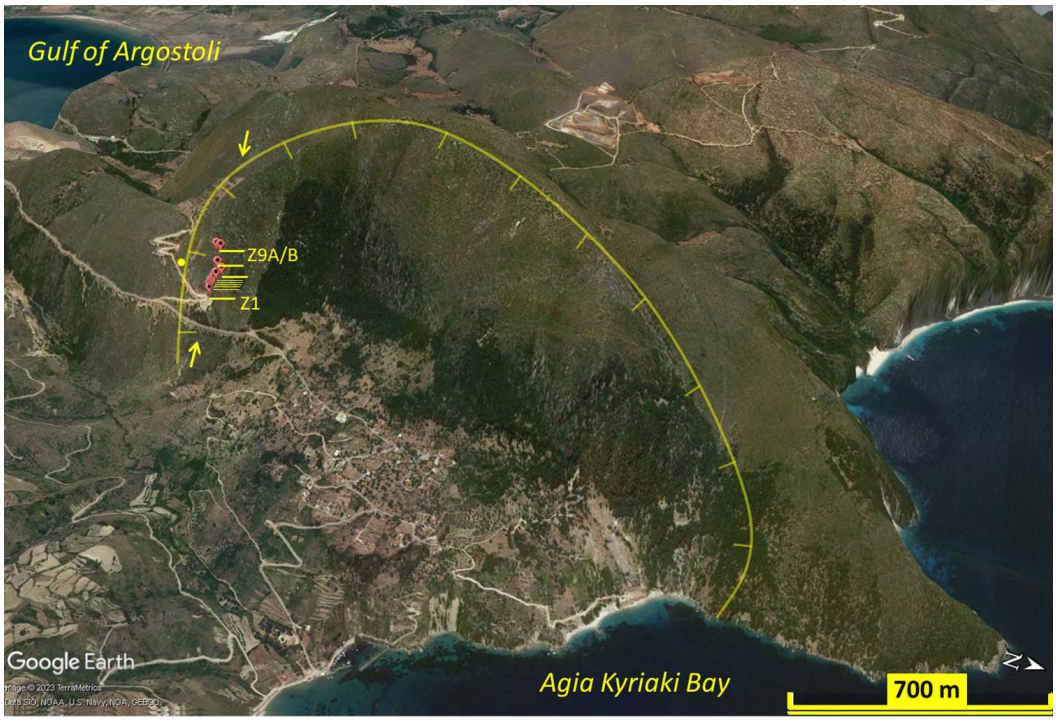

Figure 6. The distribution of samples on the southern (left) flank of the Zola landslide. Ticks perpendicular to the yellow line (crown of the landslide) are marking the concave break of the slope. The yellow dot (left of the samples) corresponds to a cluster of three samples collected outside the rim of the landslide (see Table 1). The north arrow is shown in the bottom-right corner. Basemap: Google Earth.

West of the Thinia Valley, the Aenos thrust sheet is characterized by sub-parallel, NE-SW trending elongated basins, divided by similarly trending ridges. Jenkins [25] identifies normal, NE-SW trending faults cutting through the Aenos sheet near the western fringes of the Aenos Thrust (towards the Thinia Valley) which could be interpreted as the result of accommodation to the growth of a buried culmination [3]. Nevertheless, most available geological maps, such as those by British Petroleum Company [64] or the Geological Map of Greece (Sheet: Island of Kefalonia Northern and Southern Section, scale 1:50,000, Institute of Geological and Mineral Research - IGME), simply label them as faults without specifying the sense of motion. In the field, the charted faults are associated to basinward-dipping slopes with a northwest aspect, varying from abrupt to more gently inclined. However, within a topography aged by physical erosion, it is ambiguous whether they have accommodated any sliding. With further cliff-line evolution evidence of sliding may have become indiscernible. Cliff characterization in the area is generally rather ambiguous. Such a slope, located at the southwest end of the valley (Figure 7) was selected for investigation. The toe of the slope causes the streambed to deflect sinusoidally (Figures 7 and 8).

Preprints.org (www.preprints.org) | NOT PEER-REVIEWED | Posted: 6 January 2025 doi:10.20944/preprints202501.0414.v1

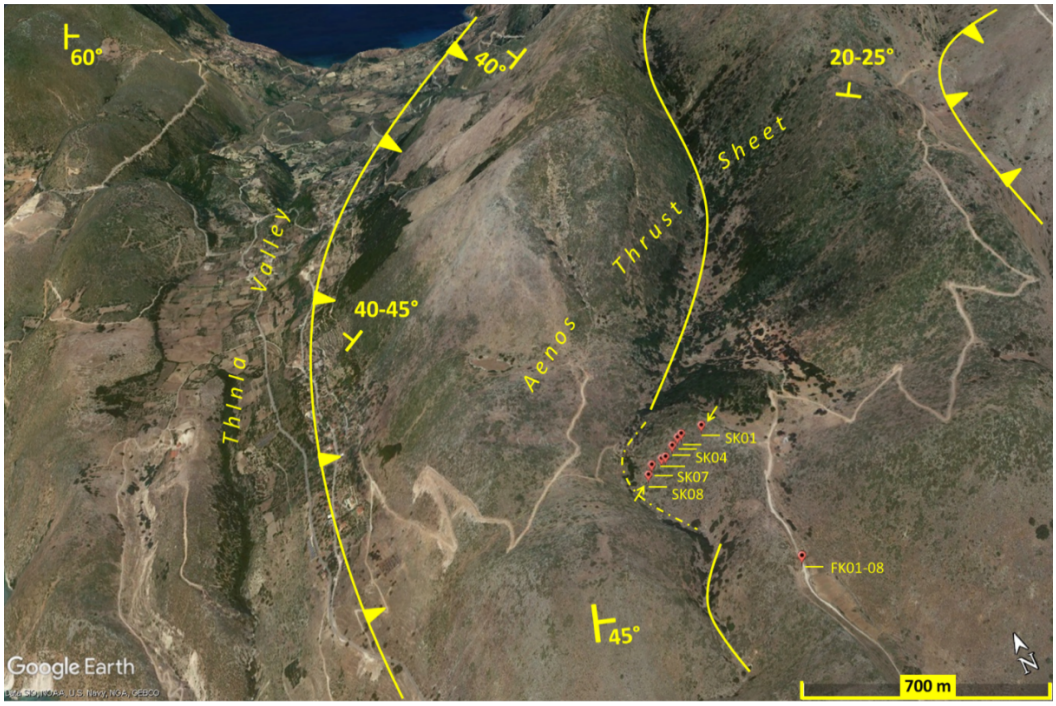

Figure 7. General view from above (looking north) showing the main tectonic lines and the Thinia Valley. The second sample site is located in the central-east part of the image. Sample positions (SK01-SK08) are marked with red pins, while a separate pin south of the studied landform marks the sampled fault plane (FK01-08). Basemap: Google Earth. The Zola landslide is situated at the northwest tip of the valley. Base map: Google Earth.

Generally, the carbonate rocks around this site are affected by joints and short normal faults. South of the landform under study at this site a 1.20 cm high, dip-slip planar surface was noticed (Figures 8 and 9), vertically offsetting the ground surface by several decimeters. Planar surfaces with such sense of motion may not be unusual in an overall compressive regime but are poorly systematic. Such structures form where compressive strain drops [65]. It is, therefore expected that the fault plane moves in tandem with the dynamic deformation of the local hanging-wall (Figure 7).

There are two approaches for carrying out exposure dating in the context of land-slipped escarpments [55]: dating the faces of scarps or dating blocks found within debris lobes. These methods both hold the potential to provide the age at which the landslide detached from its source area. However, various factors can introduce biases into exposure ages within these environments. When dating scarp faces, there is a risk of overestimating the landslide's age if the sampled surface is shallow (see the issue of inheritance addressed later). Conversely, if the sampled rock surface has weathered substantially, the estimated deposition age would again be underestimated. On the other hand, exposure ages for blocks originating from the surface may also appear older than they actually are. Blocks within or atop of debris lobes may have undergone post-deposition movement, or they might have been unearthed from beneath the original surface of the debris.

Sampling escarpments, particularly when there is reliable evidence of in situ rock slip surfaces, offers the advantage of continuous exposure in a consistent geometry. Bedrock samples (Z1 – Z09A/B, Table 1) were collected at increasing heights along a traverse on the eastern limb of the anticline (Figures 3, 5 and 6) which marks the western boundary of the Thinia Valley. All come from an exhumed face scarp flanking the Zola landslide to the south and formed in the Cretaceous carbonate bedrock (Figure 10).

 doi:10.20944/preprints202501.0414.v1

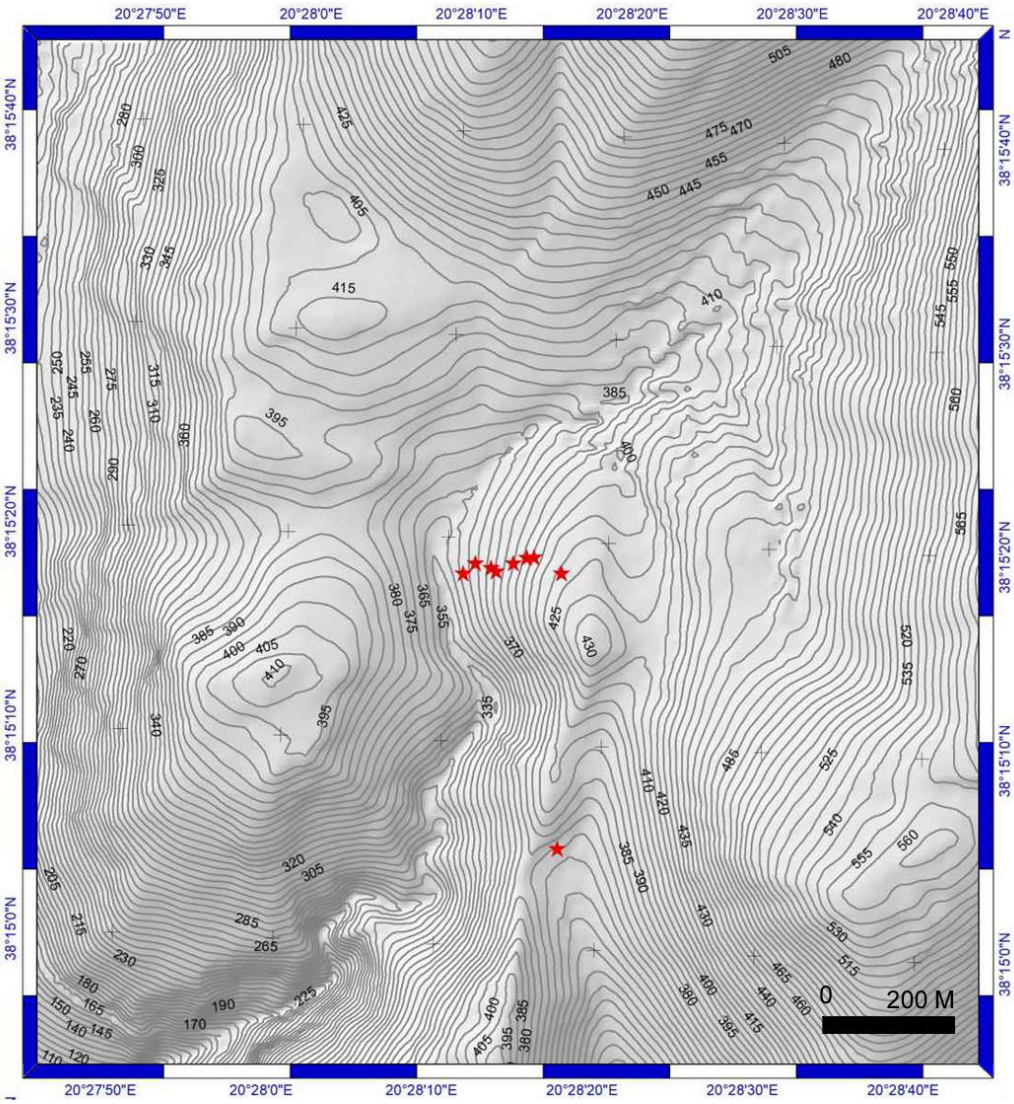

Figure 8. Topographic map of the Kourouklata area. The cluster of red stars in the middle represents the sample locations (starting with SK01 on the right and progressing sequentially to SK08 on the left), while the isolated star to the south represents the sampled fault plane (FK samples).

Perhaps, determination of age might help slope characterization at the southwestern site as well. The gently dipping surface designated in Figures 7 and 8 was sampled (SK01-SK08) along a more-or-less E-W traverse. Regarding the fracture plain south of the traverse (Figures 7–9), each time it (seismically) slips the lower segment of the plane becomes exposed to the cosmic radiation and it starts to accumulate cosmogenic ^{36}Cl. Therefore, the concentration of cosmogenic ^{36}Cl increases both with exposure time and height, serving as a proxy of the rate of tectonic slip [44,46,48,49,52] and, by implication, of upward growth of the local topography. Absence of pits and gullies on the planar surface suggests insignificant denudation. Eight (FK01-FK08) rectangular (5 cm high x 15 cm long x 2.5 cm thick) tiles were cut out along a single, continuous, base-to-top, profile parallel to the fault dip direction (Figure 9) using a cutting wheel. Spatial information of the collected samples is provided in Table 1.

 doi:10.20944/preprints202501.0414.v1

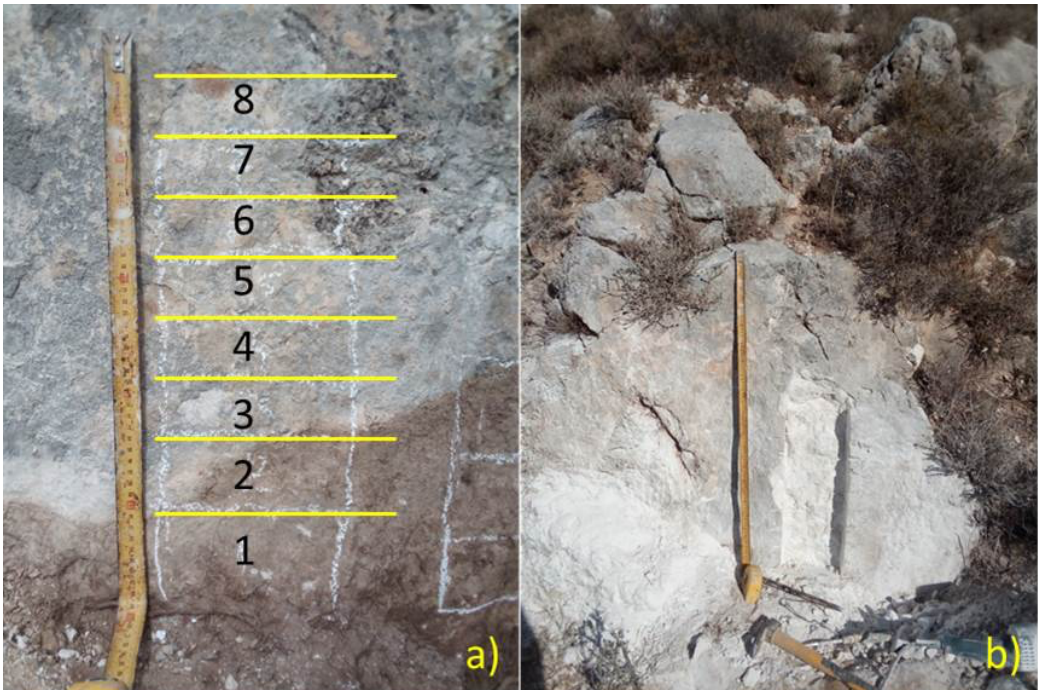

Figure 9. a) The fracture planar surface in the vicinity of the Kourouklata landform and the samples, extracted by tile-cutting wheel in 5 cm intervals. The surface is about 1 m high. b) The planar surface after the samples were cut out.

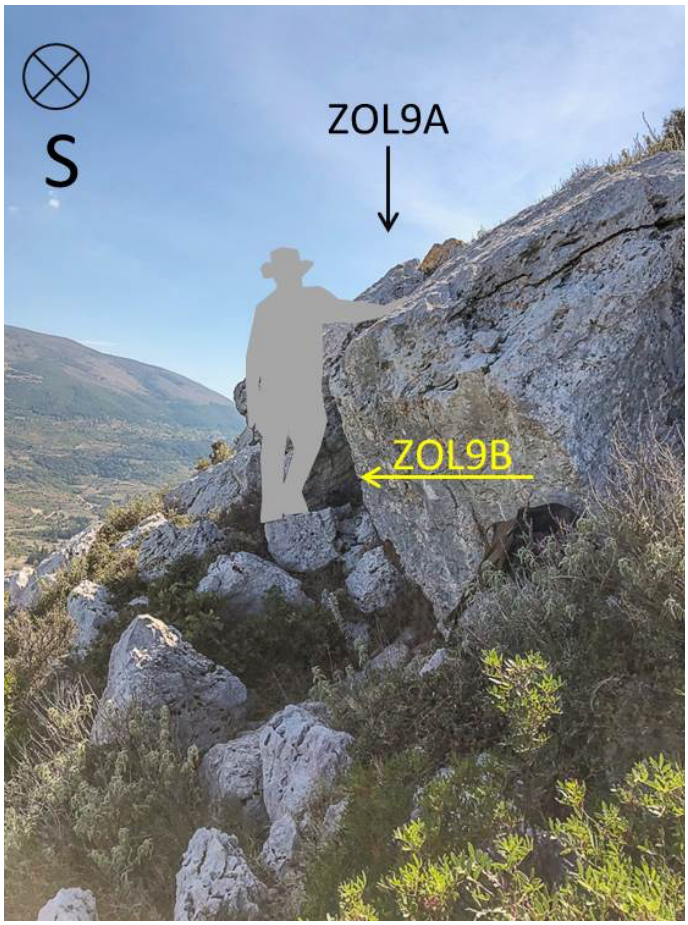

Figure 10. Sampling at position ZOL9 (below the crown of the Zola landslide). ZOL9A comes from the original surface while ZOL9B comes from an exhumed surface.

 doi:10.20944/preprints202501.0414.v1

3. Methodology

The concentrations of cosmogenic ^{36}Cl in these carbonate samples were measured to estimate cosmic ray exposure (CRE) ages and to decipher the exposure history of the landforms. The accumulation of terrestrial cosmogenic nuclides on eroding rock surfaces can be described by the following generalized equation adapted from [66]:

$$C(t) = C_{in}e^{-\lambda t} + \sum_{1}^{i} \frac{P_i}{\lambda + \rho\varepsilon/\Lambda_i}\left(1 - e^{-(\lambda+\frac{\rho\varepsilon}{\Lambda_i})t}\right) \quad (1)$$

In this equation $\boldsymbol{C(t)}$ represents the concentration of a specific cosmogenic nuclide (here ^{36}Cl) at time $\boldsymbol{t}$ in years. $\boldsymbol{i}$ denotes the type of production pathway (e.g. spallation, thermal and epithermal neutron capture, fast muons, slow muon capture). $\boldsymbol{C_{in}}$ is the concentration of any inherited amount of the nuclide resulting from previous exposures. $\boldsymbol{P_i}$ stands for the surface production rate through pathway $\boldsymbol{i}$ (measured in atoms g^{-1}a^{-1}). $\boldsymbol{\lambda}$ represents the decay constant a^{-1} if the nuclide is radioactive. $\boldsymbol{\Lambda_i}$ is the attenuation length of production pathway $\boldsymbol{i}$ (gcm^{-2}), representing the thickness of rock necessary to attenuate the cosmic-ray flux intensity by a factor of $\boldsymbol{e^{-1}}$. $\boldsymbol{\varepsilon}$ signifies the denudation rate (cm a^{-1}). After determining production rates from all pathways for a specific nuclide, Eq.1 can be solved for $\boldsymbol{t}$ to determine the exposure age to cosmic rays. In surface rocks, the production of cosmogenic ^{36}Cl occurs through spallation caused by high-energy neutrons (10-103 MeV) interacting with target elements such as Ca, K, Ti and Fe, along with the capture of low-energy (thermal and epithermal) neutrons (0.025-100 MeV) by ^{35}Cl. Additionally, the capture of slow negative muons by Ca and K yields a smaller fraction of ^{36}Cl compared to that generated by the neutron flux at the Earth's surface. Furthermore, fast muons generate energetic bremsstrahlung gamma radiation as they decelerate in matter, which can lead to the disintegration of nuclei and the release of neutrons. If these neutrons are thermalized, they can be absorbed by atoms to produce ^{36}Cl [67,69].

To solve equation (1) has to make some assumptions to determine the exposure time t (assuming denudation is known) or to quantify the denudation rate ε (assuming steady state). To date as accurately as possible landsliding events, a serious issue which should not be overlooked while estimating cosmogenic ages is inheritance [52,55,56,58,61,70]. Prior to bedrock exhumation the topography is constantly showered by cosmic rays which penetrate the bedrock for several meters. Therefore, the production of the TCN persists to some depth while diminishing exponentially along the way. After a new surface cuts through the topography (i.e. landslide escarpment or fault plane), the isotopes previously generated are inherited to the freshly exposed surface and are supplemented by the newly accumulating ^{36}Cl inventory. To estimate the concentration of inherited nuclides at depth, it is imperative to constrain the local long-term denudation rate affecting the terrain. The inheritance factor is theoretically influenced by three main variables: 1) the extended surface denudation rate, representing erosion from above, 2) the depth beneath the surface, and 3) the material density [66].

A simplistic exposure model could have been employed, factoring in only the topographic shielding and latitudinal scaling of cosmic ray flux. Nevertheless, when considering the extension of the initial topographic surface in relation to the landslide escarpment surface resulting from in the DEM (Figure 5) thinner exhumation should be acknowledged, particularly in higher elevations. This underscores the necessity for adaptations in nuclide production at shallow depths preceding the exhumation process. The pre-exposure depth of the samples was therefore estimated relative to that level, with the understanding that it naturally increased downslope.

The carbonate samples were chemically processed according to standard procedures [43,57,58,70]. The quantification of cosmogenic ^{36}Cl concentrations involved accelerator mass spectrometry (AMS) measurements conducted at ASTER, the French national AMS facility located at CEREGE in Aix-en-Provence, following the methodology outlined by Arnold et al. [71].

 doi:10.20944/preprints202501.0414.v1

4. Results

For each site, the denudation rate (normally the lower denudation rate) of the topmost surface sample (referred as reference sample, Z06, SK01 and FK01 respectively) has been considered to determine the inheritance at depth of the other samples. To do so, the time is set at infinite (steady state) and the inheritance is determined by subtracting the estimated inherited nuclide concentration at its original depth (prior to the land sliding event) from the measured ^{36}Cl (Table 1, column 5).

The production rate of ^{36}Cl through calcium spallation at sea level and high latitudes was determined as 42.2 ± 3.4 atoms ^{36}Cl g^{-1} atoms^{-1} as per Schimmelpfennig et al. [72] and Braucher et al. [73]. This rate was scaled using the approach proposed by Stone [68] and corrected for topographic shielding, which was derived from the high-resolution digital elevation model using the algorithm of Ying-kui [74]. For a comprehensive understanding of the dating method and analytical procedures, the reader is encouraged to refer to previous studies [70,75,76]. Initially, all exposure times were determined considering the sampling depth without denudation and inheritance correction (min age, Table 1). Then the exposure times were set to infinite to determine the maximum denudation rate for each sample at the sampling depth (max. den., Table 1). Afterwards, for each site the lower maximum denudation rate was used to determine the inherited component for each sample assuming the depth prior the sliding event. This step is crucial for the determination of the inheritance at depth. Finally, for each sample the inheritance-corrected exposure age is obtained (Table 1, last column). The assumptions underlying the estimation of inheritance assume that the concave escarpment, prior to landsliding, was covered by a parcel of rock, which once extended across the imagined continuation of the contemporary original surface.

The ages calculated for all samples from both sites are shown in Table 1. All exposure ages are expressed as *ka ago*. Those designated as *steady state* represent landform segments in which the contribution rate to the cosmogenic ^{36}Cl budget by nuclear interactions was found to be canceled by the nuclide loss rate due to erosion for the given parameters (scaled production rate and denudation). Therefore, for these samples only minimum ages can be considered (Table 1, column 9). Setting aside those associated with steady state, the rest of the exposure ages extend from the Middle Pleistocene through the Holocene to historical times. Samples Z10A, Z10B and Z02B2 do not come from the sampled traverse but constitute a cluster of samples collected from the bedrock ~ 200 m away from the rim of the Zola landslide (yellow point in Figure 6).

They exhibit rather (unusually) high denudation rates (Table 1, column 10) raising cautiousness as to their exposure history. Given their proximity to road cuts (Figures 5 and 6) there is a concern that these three samples may have been artificially disturbed, potentially resulting in partial reset of their ^{36}Cl budget. This potential scenario calls for caution regarding the usefulness of these three samples for further geochronological implications.

At the second study site half of the exposure ages (SK01,2,4,5,8) imply steady-state conditions, whereas the rest suggest a distal age between 40 and 60 ka, but lacking any discernible directional pattern. Finally, the uppermost levels of the nearby short fault plane located south of were found to be in steady state (which is reasonable given their shallow depth below the aforementioned surface) while the remaining, deeper, samples yielded cosmogenic ^{36}Cl exposure ages (Table 1) which cluster around ~ 4.3 ± 0.7 ka without showing any decrease in age with depth, indicative of recurrent slip such the fashion shown elsewhere [44,46].

Table 1. Spatial information of the collected samples, , ^{36}Cl and ^{56}Cl concentrations, concentration of Ca, topographic shielding (using the method by Ying-kui [74]), minimum ages and exposure ages calculated with denudation. Ages marked by an asterisk come from the current topographic surface south of the landslide. Given their substantially high associated denudation rates compared to the one of the reference sample, it is preferred that only the associated minimum ages are considered.

Sample	Lat.	Long.	Elev.	^{36}Cl	^{35}Cl	%Ca	Topo	Min age (no	Max. denud.	Denudation of	Exposure age

 doi:10.20944/preprints202501.0414.v1

								denudation)		ref sample	
			(m a.s.l.)	(at/g)	(ppm)	Shielding		(ka)	(m/Ma)		(ka)
SK01	38.25776969	20.47303338	404	735717 ± 33685	2	39.359	0.9956	25.32 ± 1.16	42.83 ± 1.96	40.00	236.42 ± 10.82
SK02	38.25797481	20.47255184	389	715670 ± 32515	10	40.090	0.9898	21.26 ± 0.97	49.59 ± 2.25	40.00	105.37 ± 4.79
SK03	38.25796523	20.47242618	386	549114 ± 25545	8	40.139	0.9888	16.53 ± 0.77	65.66 ± 3.05	40.00	39.23 ± 1.83
SK04	38.2578831	20.47219818	378	741515 ± 81627	44	40.784	0.9880	24.95 ± 2.75	46.58 ± 5.13	40.00	151.68 ± 16.7
SK05	38.2577646	20.47190186	371	738992 ± 33517	29	40.022	0.9885	22.87 ± 1.04	47.72 ± 2.16	40.00	128.44 ± 5.83
SK06	38.25780925	20.47181009	367	576172 ± 26005	42	39.722	0.9887	20.21 ± 0.91	59.19 ± 2.67	40.00	60.77 ± 2.74
SK07	38.25786209	20.47153539	358	513814 ± 22757	22	39.825	0.9893	18.67 ± 0.82	63.78 ± 2.82	40.00	49.35 ± 2.19
SK08	38.25771697	20.47133071	351	658402 ± 29933	20	40.013	0.9881	22.93 ± 1.04	49.45 ± 2.25	40.00	116.9 ± 5.31
FK01	38.25771697	20.47133071	366	306710 ± 18086	103	25.111	0.9813	13.61 ± 0.80	95.59 ± 5.64	95.59	5.23 ± 0.31
FK02	38.25409336	20.47319708	366	295629 ± 16159	89	26.075	0.9813	12.86 ± 0.70	99.51 ± 5.44	95.59	4.89 ± 0.27
FK03	38.25409336	20.47319708	366	265267 ± 15606	94	24.765	0.9813	12.18 ± 0.72	107.67 ± 6.33	95.59	4.28. ± 0.25
FK04	38.25409336	20.47319708	366	268455 ± 16396	94	25.808	0.9813	11.50 ± 0.70	111.76 ± 6.83	95.59	4.39 ± 0.27
FK05	38.25409336	20.47319708	366	262391 ± 14733	92	25.833	0.9813	11.22 ± 0.63	114.86 ± 6.45	95.59	4.77 ± 0.27
FK06	38.25409336	20.47319708	366	260559 ± 18793	101	25.257	0.9813	11.06 ± 0.80	117.36 ± 8.46	95.59	5.05 ± 0.36
FK07	38.25409336	20.47319708	366	222756 ± 14504	81	26.201	0.9813	9.07 ± 0.59	137.30 ± 8.94	95.59	3.11 ± 0.20
FK08	38.25409336	20.47319708	366	238940 ± 13327	77	27.776	0.9813	9.21 ± 0.51	133.18 ± 7.43	95.59	4.09 ± 0.23
Z01	38.30197617	20.46523406	216	363183 ± 16172	11	39.757	0.9683	12.38 ± 0.55	91.75 ± 4.09	50.00	25.64 ± 1.14
Z01A	38.30197617	20.46523406	224	160642 ± 8258	17	39.809	0.9673	5.43 ± 0.28	219.29 ± 11.27		*5.43 ± 0.28
Z01B	38.30197617	20.46523406	224	156448 ± 7919	17	39.717	0.9673	6.41 ± 0.33	202.96 ± 10.27		*6.41 ± 0.33
Z02	38.30195767	20.46513126	218	355935 ± 16680	32	39.818	0.9703	14.16 ± 0.66	88.68 ± 4.16	50.00	31.94 ± 1.50
Z02B	38.30195767	20.46513126	230	135209 ± 9677	21	39.784	0.9657	8.72 ± 0.62	194.58 ± 13.93	50.00	11.79 ± 0.84
Z02B2	38.30195767	20.46513126	230	109344 ± 6505	21	39.800	0.9657	4.16 ± 0.25	307.60 ± 18.30		*4.16 ± 0.25
Z03	38.30197528	20.46503964	233	293212 ± 13239	14	39.934	0.9622	10.99 ± 0.50	110.13 ± 4.97	50.00	19.28 ± 0.87
Z04	38.3020292	20.46500493	237	630575 ± 28345	28	39.774	0.9616	21.61 ± 0.97	51.65 ± 2.32	50.00	265.26 ± 11.92

 doi:10.20944/preprints202501.0414.v1

Z05	38.30205592	20.46493612	238	341582 ± 15298	24	39.791	0.9608	13.61 ± 0.61	91.90 ± 4.12	50.00	29.49 ± 1.32
Z06	38.3020915	20.46483292	244	628376 ± 28353	27	39.911	0.9580	23.51 ± 1.06	49.16 ± 2.22	50.00	Steady state
Z07	38.30225304	20.46468306	252	522870 ± 23515	26	39.034	0.9567	23.86 ± 1.07	52.63 ± 2.37	50.00	237.16 ± 10.67
Z08	38.30208123	20.46455852	255	535861 ± 25708	15	39.508	0.9614	24.38 ± 1.17	50.70 ± 2.43	50.00	359.11 ± 17.23
Z09A	38.30207029	20.46413543	282	775022 ± 35348	27	39.855	0.9591	34.18 ± 1.56	34.83 ± 1.59	34.83	Steady state
Z09B	38.30192604	20.46412506	281	428512 ± 19142	13	40.040	0.5000	32.23 ± 1.44	51.37 ± 2.29	34.83	1.43 ± 0.64

5. Discussion

The exposure ages reported here provide the first direct estimates of the timing of landscape evolution and ground deformation in the Ionian Islands. At the first study site around Zola the exposure ages demonstrate that ground deformation on the eastern limb of the associated anticline has been ongoing since at least the Middle Quaternary to historical times as the ages span between 359 and 1.4 ka over which the spread of the ages suggests (Z1-Z09A/B). Despite the observation that the exposure age generally tends to increase uphill, occasional drops in the same direction are evident (Figure 11): old ages intermingle with young (even historical, around 1.5 ka ago) ones. Three of the older ages (Z04,8,9) may be identified with a residual terrain dating to the Middle Pleistocene (237-359 ka). This timeframe likely marks the exhumation of the wider escarpment which is crowned by the long cliff high up the escarpment (Figures 5 and 6). Interruptions by distinctively younger exposure ages at around 32, 30, 19, 12, 1.7 and 1.4 ka may imply a more complex ground deformation history of the Zola landslide.

The presence of distinctly younger segments of mass wasting within the principal (relict) surface distributed over tens of thousands of years rather than caused by a single catastrophic event is a pattern of exhumation that has also been demonstrated elsewhere by recent similar studies which were benefited from cosmogenic nuclides [56,61,70,77].

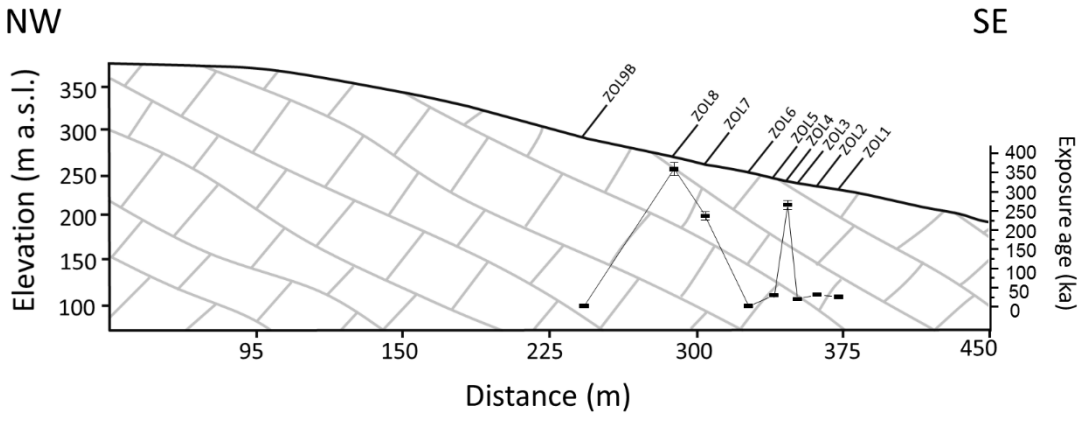

Figure 11. Spatial (1D) distribution of the cosmogenic ^{36}Cl ages along the sampled topographic profile. Note the different scale on the axis on the left. Bedding dip ~ 60°. The cosmogenic 14Cl exposure age per sample is shown on the y axis on the right. The profile is contained between the two yellow arrows shown in Figure 6.

The exposure ages indicate that ground deformation on the eastern limb of the associated anticline has been ongoing since at least the Middle Quaternary, continuing nearly to the present. This brings us back to the initial question: an anticline is present in which the eastern limb has been

 doi:10.20944/preprints202501.0414.v1

collapsing since at least the Middle Pleistocene, while no evidence of (equally intense) ground deformation could be documented for the western limb.

The ENE dips (50°-60°) are steeper than the westerly ones (~30°), as shown in Figure 4, and this creates more favorable conditions for failure in the Thinia Valley. Rises in temperature and precipitation are considered crucial in triggering slope failure. Therefore, it is not surprising that many recent large-scale landslides, particularly in the Alpine belt, coincide with the beginning of the Holocene epoch (see above references). Indeed, the Holocene period is characterized by a significant warming and increased precipitation after deglaciation, which played a pivotal role in initiating and exacerbating slope failures. During periods of uncertain climatic factors, enhanced seismic activity in the Ionian Islands is a possible factor of causing deterioration in the mechanical characteristics of the bedrock more significantly than external factors. Failure mechanisms are initiated along planes of weakness (primarily bedding). Regional earthquakes appear powerful enough to trigger landslides. These arguments sufficiently explain the translational component of slope failure in the Thinia Valley. Careful observation of the available aerial imagery (Figure 5b) reveals not only translational components but also longitudinal ruptures deeper seated (possibly listric) into the bedrock with normal sense of motion—a pattern of ground deformation that cannot be explained solely by climatic influences or co-seismic superficial mass-wasting processes and block translation but more as a structural response to the growth of a buried culmination [3].

Hermanns et al. [33,34] and Strecker and Marrett [35] showed that the frequency and location of landslides linked to reverse faults in mountain ranges (Andes) shifts in tandem with the locus of compression. Explicit events of landsliding occured 400 ka ago and repeated with a 30 ka cyclicity until 150 ka, when it is assumed that the locus of tectonic deformation migrated farther away in the Andean foreland. It also appears that folding in northern Kefalonia is primarily driven through thrust-fault bend folding [3,25]. The compression-induced asymmetry in the Zola anticline's dip makes the eastern limb more susceptible to landsliding.

Additional evidence comes from the Copernicus European Ground Motion Service (EGMS). Velocity markers on the thrust sheet east of the Thinia Valley show an almost uniform westerly velocity component of 7-8 $mm \cdot y^{-1}$. However, on the eastern limb of the said anticline, around the Zola landslide, the westerly velocity decreases over a distance of 2 km, with multiple markers on this limb showing velocities less than 3 $mm \cdot y^{-1}$. Could this apparent deceleration –nearly halved within such a short distance– be interpreted as a resultant motion, where the relative velocity of the faster moving foreland combines with that of an eastern limb deforming eastward, resulting in slower net forward movement in the foreland's direction? In this scenario the eastern limb of the anticline could be serving as the active limb of the anticline making it, thus, susceptible to ongoing ground deformation due to the redistribution of its rock mass through deep-seated breakdown. Should these hypotheses hold, they suggest that we may be observing a tectonically mobile mountain which was began evolving at least in the Middle Pleistocene, as implied by the current cosmogenic ^{36}Cl dating, and may still be active. Nonetheless, additional structural data are required to confirm these interpretations.

However, for the secondary site most of the cosmogenic ^{36}Cl dates reflect a surface in steady state (Table 1), meaning that in-situ production of cosmogenic ^{36}Cl is balanced by ^{36}Cl loss due to radioactive decay and surface erosion. Hence, the current results (Table 1) should only be treated as minimum values implying that the said surface should be at least Middle- Pleistocene in age. Previous drilling campaigns north of the site at 107 m a.s.l. retrieved loose rockfall down to 15 meters below sea level running north to south [40,41]. Notably, the marine microfossil *Emiliania huxleyi* was discovered mixed with older loose rockfall sediments within the top 40 meters of the borehole [40,41]. Additionally, gravity lines positioned across the eastern side of the valley have revealed some negative Bouguer anomalies, indeed suggesting the presence of buried rockfall. This indicates that the eastern slopes of the Thinia valley predominantly consist of low density materials such as rockfall debris [40]. Nevertheless, a few exceptions (SK03,6,7) are statistically too small to illuminate the origin of the surface. Constraining the age of this topographic surface may lie beyond the range of

 doi:10.20944/preprints202501.0414.v1

cosmogenic - ^{36}Cl dating but, be that as it may, the small fault escarpment that cuts the studied surface to the south shows evidence of very recent activity in the vertical sense. If the fault plane motion is correlated with the local deformation then so is the chronology of the kinematic and dynamic growth of the local bedrock. A tectonically co-seismic vertical offset ~ 4.3 ± 0.7 ka ago may indicate recent dynamic growth of the bedrock.

6. Conclusions

The cosmogenic ^{36}Cl exposure ages from this study provide the first direct chronology of landscape evolution and ground deformation in the Ionian Islands, specifically in the Thinia Valley and the anticline near Zola in northern Kefalonia. At the first study site, Zola, the exposure ages demonstrate that deformation on the eastern limb of the anticline extends from the Middle Quaternary to historical times. This wide chronological span, with a complex mix of ancient and younger ages, suggests that the anticline has been affected multiple ground deformation events rather than a single episode. Older ages align with a Middle Pleistocene phase of exhumation while younger exposure ages point to additional mass-wasting events likely driven by both climatic shifts and tectonic influences. This suggests that in northern Kefalonia, tectonic strain continues to vertically redistribute the bedrock—a process that has likely been active since at least the Middle Pleistocene and may still be ongoing. This underscores its importance for hazard assessment and highlights the dynamic nature of a landscape being shaped by tectonic forces. However, additional structural data are required to confirm of alter the interpretation.

At the second site, Kourouklata, the exposure ages indicate a steady-state surface, where erosion and radioactive decay balance the production of cosmogenic ^{36}Cl providing only minimum age estimates. This suggests that the true age of the surface may lie beyond the reach of cosmogenic dating, leaving the origin of the slope uncharacterized. Nonetheless, recent tectonic activity on a fault cutting through this surface as indicated by ^{36}C dating points to an actively evolving tectonic landscape persisting into the Holocene.

Author Contributions: Conceptualization, CDA; methodology, RB and CDA; fieldwork, CDA; DEMs and map rendering in GIS environment, IV; investigation, CDA; data curation, CDA and RB; writing—original draft preparation, CDA; writing—review and editing, CDA, RB; academic outreach, GA.

Funding: Please add: Fieldwork and dating of the samples was funded by the Odysseus Unbound Foundation (OUF).

Data Availability Statement: We encourage all authors of articles published in MDPI journals to share their research data. In this section, please provide details regarding where data supporting reported results can be found, including links to publicly archived datasets analyzed or generated during the study. Where no new data were created, or where data is unavailable due to privacy or ethical restrictions, a statement is still required. Suggested Data Availability Statements are available in section "MDPI Research Data Policies" at https://www.mdpi.com/ethics.

Acknowledgments: Prof. J. R. Underhill (Aberdeen University, Scotland, UK) and Prof. P. Styles (Keele University, England, UK) are gratefully thanked for introducing the authors to the Thinia Valley and Zola landslide and an exchange of valuable ideas in the field and when conceiving the paper. ASTER AMS, national facility (CEREGE, Aix en Provence), is supported by the INSU/CNRS and IRD and member of AIX MARSEILLE PLATFORMS and REGEF networks. Aster Team (G. Aumaître, K. Keddadouche, F. Zaïdi) is acknowledged for the AMS measurements.

Conflicts of Interest: The authors declare no conflicts of interest.

References

1. McKenzie, D. P. 1978. Active tectonics of the Alpine-Himalayan belt: the Aegean Sea and surrounding regions, *Geophys. J. R. astr. Soc*., 55, 217-254.

 doi:10.20944/preprints202501.0414.v1

2. Le Pichon, X., Lyberis. N., Angelier, J., Renards, V. 1982. *Tectonophysics*, 243-274.
3. Underhill, J. R. 1989. Late Cenozoic Deformation of the Hellenic Foreland, Western Greece. *Geological Society of America Bulletin*, 101, 613-634.
4. Royden, L.H. 1993. The tectonic expression slab pull at continental convergent boundaries. *Tectonics*, 12, 303-325
5. Louvari, E., Kiratzi, A.A., Papazachos, B.C. 1999. The Cephalonia transform fault and its extension to western Lefkada Island (Greece). Tectonophysics, 308, 223–236.
6. Özbakir, A.D., Govers, R., Fichtner, A. 2020. The Kefalonia Transform Fault: A STEP fault in the making. *Tectonophysics*, 787, 228471
7. Baker, C., Hatzfeld, D., Lyon-Caen, H., Papadimitriou, E., Rigo, A. 1997. Earthquake mechanisms of the Adriatic Sea and Western Greece: Implications for the oceanic subduction-continental collision transition. *Geophysical Journal International*, 131, 559-594
8. Papadimitriou, E.E. 2002. Mode of strong earthquake recurrence in the central Ionian Islands (Greece): Possible triggering due to Coulomb stress changes generated by the occurrence of previous strong shocks. *Bull. Seismol. Soc. Am*. 92, 3293-3308,
9. Papazachos, C.B., Kiratzi, A.A. 1996. A detailed study of the active crustal deformation in the Aegean and surrounding area. Tectonophysics,253, 129-153
10. Kahle, H.G., Müller, M.V., Geiger, A., Danuser, G., Mueller, S., Veis, G., Billiris, H., Paradissis, D. 1995. The strain field in northwestern Greece and the Ionian Islands: Results inferred from GPS measurements. Tectonophysics, 249, 41–52
11. Cocard, M., Kahle, H.G., Peter, Y., Geiger, A., Veis, G., Felekis, S., Paradissis, D., Billiris, H. 1999. New constraints on the rapid crustal motion of the Aegean region: Recent results inferred from GPS measurements (1993–1998) across the West Hellenic Arc, Greece. Earth Planet. Sci. Lett., 172, 39–47.
12. Kourouklas, C., Papadimitriou, E., Karakostas, V. 2023. Long-Term Recurrence Pattern and Stress Transfer along the Kefalonia Transform Fault Zone (KTFZ), Greece: Implications in Seismic Hazard Evaluation. *Geosciences*, 13, 295.
13. Scordilis, E., Karakaisis, G.F., Karakostas, V., Panagiotopoulos, D.G., Comninakis, P.E., Papazachos, B.C. 1985. Evidence for Transform Faulting in the Ionian Sea: The Cephalonia Island earthquake sequence of 1983. Pure Appl. Geophys., 123, 388–397.
14. Kiratzi, A., Langston, C. 1991. Moment tensor inversion of the 1983 January 17 Kefallinia event of Ionian Island (Greece). Geophys. J. Int., 105, 529–538
15. Papadimitriou, E. 1993. Focal mechanisms along the convex side of the Hellenic Arc. Boll. Geof. Teor. Appl., 140, 401–426.
16. Triantafyllou, I., Papadopoulos, G.A. 2023. Earthquakes in the Ionian Sea, Greece, Documented from Little-Known Historical Sources: AD 1513–1900. Geosciences, 13, 285.
17. Pirazzoli, P., Stiros, S., Laborel, J., Laborel-Deguen, F., Arnold, M., Papageorgiou, S., Morhangel, C. 1994. Late-Holocene shoreline changes related to palaeoseismic events in the Ionian Islands, Greece. Holocene, 4, 397–405.
18. Stiros, S., Pirazzoli, P.A., Laborel, J., Laborel-Doguen, F. 1994. The 1953 earthquake in Cephalonia (Western Hellenic Arc): Coastal uplift and halotectonic faulting. Geophys. J. Int., 117, 834–849
19. Rondoyianni, T., Sakellariou, M., Baskoutas, J., Christodoulou, N. 2012. Evaluation of active faulting and earthquake secondary effects in Lefkada Island, Ionian Sea, Greece: an overview, Natural Hazards, 61, 843-850
20. Papadopoulos, G.A., Karastathis, V.K., Koukouvelas, I., Sachpazi, M., Baskoutas, G., Agalos, A., Daskalaki, E., Minadakis. G., Moshou, A., Mouzakiotis, A., Orfanogiannaki, K., Papageorgiou, A., Spanos, D., Triantafyllou, I. 2014. The Cephalonia, Ionian Sea (Greece), sequence of strong earthquakes of January–February 2014: a first report. Res Geophys. doi:10.4081/rg.2014.5441
21. Lekkas, E.L., Mavroulis, S.D. 2014. Earthquake environmental effects and ESI 2007 seismic intensities of the early 2014 Cephalonia (Ionian Sea, Western Greece) earthquakes (January 26 and February 3, Mw 6.0). Nat. Hazards, 78, 1517–1544

 doi:10.20944/preprints202501.0414.v1

22. Valkaniotis, S., Ganas, A., Papathanasiou, G., Papanikolaou, M. 2014. Field observations of geological effects triggered by the January–February 2014 Cephalonia (Ionian Sea, Greece) earthquakes. Tectonophysics, 630, 150 -157
23. Mavroulis, S., Lekkas, E. 2021. Revisiting the Most Destructive Earthquake Sequence in the Recent History of Greece: Environmental Effects Induced by the 9, 11 and 12 August 1953 Ionian Sea Earthquakes. Appl. Sci. 2021, 11, 8429. https:// doi.org/10.3390/app11188429
24. Mavroulis, S., Diakakis, M., Kranis, H., Vassilakis, E., Kapetanidis, V., Spingos, I., Kaviris, G., Skourtsos, E., Voulgaris, N., Lekkas, E. 2022. Inventory of Historical and Recent Earthquake-Triggered Landslides and Assessment of Related Susceptibility by GIS-Based Analytic Hierarchy Process: The Case of Cephalonia (Ionian Islands,Western Greece). Appl. Sci., 12, 2895.
25. Jenkins, D. A. L. 1972. Structural development of Western Greece. *AAPG Bulletin*, 56, 128–149.
26. Underhill, J.R. 1988. Triassic Evaporites and Plio-Quaternary Diapirism in Western Greece. Journal of the Geological Society of London, 145, 209-282.
27. Le Pichon, X. and Angelier, J. 1979. The hellenic arc and trench system: A key to the neotectonic evolution of the eastern mediterranean area. Tectonophysics, 60, 1-42.
28. Karakostas, V.G., Papadimitriou, E.E. and Papazachos, C.B. 2004. Properties of the 2003 Lefkada, Ionian Islands, Greece, earthquake seismic sequence and seismicity triggering, *Bull. Seismol. Soc. Am.*, 94, 1976–1981.
29. Ganas, A., Elias, P., Bozionelos, G., Papathanassiou, G., Avallone, A., Papastergios, A., Valkaniotis, S., Parcharidis, I., Briole, P. Coseismic deformation, field observations and seismic fault of the 17 November 2015 M = 6.5, Lefkada Island, Greece earthquake. *Tectonophysics*, 687, 210-222
30. Saltogianni, V., Moschas, F., Stiros, S. 2018. The 2014 Cephalonia Earthquakes: Finite Fault Modeling, Fault Segmentation, Shear and Thrusting at the NW Aegean Arc (Greece). *Pure Appl. Geophys*., 175, 4145-4164
31. Svigkas, N., Atzori, S., Kiratzi, A., Tolomei, C., Antonioli, A., Papoutsis, I., Salvi, S., Kontoes, C. 2019. On the Segmentation of the Cephalonia–Lefkada Transform Fault Zone (Greece) from an InSAR Multi-Mode Dataset of the Lefkada 2015 Sequence. *Remote Sens*., 11, 1848.
32. Royden L.H. and Papanikolaou, D.J. 2011. Slab segmentation and late Cenozoic disruption of the Hellenic arc. *Geochemistry, Geophysics, Geosystems*, *12*, Q03010
33. Hermanns, R. L., Niedermann, S., Villanueva Garcia, A., Sosa Gomez, J. and Strecker, M. R. 2001. Neotectonics and catastrophic failure of mountain fronts in the southern intra-Andean Puna Plateau, Argentina. *Geology*, 29, 619–623.
34. Hermanns, R. L. and Strecker, M. R. 1999. Structural and lithological controls on large Quaternary rock avalanches (sturzstroms) in arid northwestern Argentina. Geological Society of America Bulletin, 111, 934–948.
35. Strecker, M. R. and Marrett, R. 1999. Kinematic evolution of fault ramps and its role in development of landslides and lakes in the northwestern Argentine Andes. *Geology*, 27, 307–310.
36. Jackson, L. E., Jr. 2002. Landslides and landscape evolution in the Rocky Mountains and adjacent foothills area, southwestern Alberta, Canada. In Catastrophic Landslides, ed. S. G. Evans and J. V. DeGraff. Geological Society of America, Reviews in Engineering Geology 15, 325–344.
37. Agliardi, F., Zanchi, A. and Crosta, G. B. 2009a. Tectonic vs. gravitational morphostructures in the central Eastern Alps (Italy): Constraints on the recent evolution of the mountain range. Tectonophysics, 474, 250–270.
38. Agliardi, F., Crosta, G. B., Zanchi, A. and Ravazzi, C. 2009b. Onset and timing of deep-seated gravitational slope deformations in the eastern Alps, Italy. Geomorphology, 103, 113–129.
39. Penna, I., Hermanns, R. L., Folguera, A. and Niedermann, S. 2011.Multiple slope failures associated with neotectonic activity in the southern central Andes (37°–37°30′S). Patagonia, Argentina. *Geological Society of America Bulletin*, 123, 1880–1895.
40. Underhill, J.R. 2006. Quest for Ithaca. Geoscientist 16, 9, 4-29
41. Underhill, J. 2009. Relocating Odysseus' Homeland. Nature Geoscience, 2, 455-458
42. Oldrich, H., Leroueil, S., Picarelli, L. 2014. The Varnes classification of landslide types, an update. *Landslides*, 11, 167-194.

 doi:10.20944/preprints202501.0414.v1

43. Pérouse, E., Sébrier, M., Braucher, R., Chamot-Rooke, N., Bourles, D., Briole, P., Sorel. D., Dimitrov, D., Arsenikos, S. 2017. Transition from collision to subduction in Western Greece: the Katouna–Stamna active fault system and regional kinematics. International Journal of Earth Sciences, 2017, 106, 967-989.
44. Mechernich, S., Schneiderwind, S., Mason, J., Papanikolaou, I. D., Deligiannakis, G., Pallikarakis, A., Binnie, A.S., Dunai, T.J., Reicherter, K. 2018. The Seismic History of the Pisia Fault (Eastern Corinth Rift, Greece) from Fault Plane Weathering Features and Cosmogenic ^{36}Cl Dating. *J. Geophys. Res. Solid Earth*, 123, 4266–4284.
45. Iezzi, F., Roberts, G., Faure Walker, J., Papanikolaou, I., Ganas, A., Deligiannakis, G., Beck, J., Wolfers, S., Gheorghiu, D. 2021. Temporal and spatial earthquake clustering revealed through comparison of millennial strain-rates from ^{36}Cl cosmogenic exposure dating and decadal GPS strain-rate. *Sci Rep* 11, 23320
46. Mechernich, S., Reicherter, K., Deligiannakis, G., Papanikolaou, I. 2023. Tectonic geomorphology of active faults in Eastern Crete (Greece) with slip rates and earthquake history from cosmogenic ^{36}Cl dating of the Lastros and Orno faults. *Quaternary International*, 30, 77-91
47. Zreda, M.G., and Noller, F.M. 1998. Ages of prehistoric earthquakes revealed by cosmogenic chlorine-36 in a bedrock fault scarp at Hebgen Lake: Science, 282, 1097–1099
48. Schlagenhauf, A., Gaudemer, Y., Benedetti, L., Manighetti, I., Palumbo, L., Schimmelpfennig, I., Finkel, R., Pou, K., 2010. Using in situ chlorine-36 cosmonuclide to recover past earthquake histories on limestone normal fault scarps: a reappraisal of methodology and interpretations. *Geophys. J. Int.* 182, 36-72.
49. Mouslopoulou, V., Moraetis, D., Benedetti, L., Guillou, V., Bellier, O., Hristopulos, D. 2014. Normal faulting in the forearc of the Hellenic subduction margin: Paleoearthquake history and kinematics of the Spili Fault, Crete, Greece. *Journal of Structural Geology*, 66, 298-308
50. Benedetti, L., Finkel, R., King, G., Armijo, R., Papanastasiou, D., Ryerson, F.J., Flerit, F., Farber, D., Stavrakakis, G. 2001. Motion on the Kaparelli fault (Greece) prior to the 1981 earthquake sequence determined from ^{36}Cl cosmogenic dating. *Terra Nova*, 15, 118-124
51. Benedetti, L., Finkel, R., Papanastasiou, D., King, G., Armijo, R., Ryerson, F.J., Farber, D., Flerit, F. 2002. Post-glacial slip history of the Sparta fault (Greece) determined by ^{36}Cl cosmogenic dating: Evidence for non-periodic earthquakes. *Geophysical Research Letters*, 29, 1246
52. Benavente, C., Zerathe, S., Audin, L., Hall, S.R., Robert, X., Delgado, F., Carcaillet, J., ASTER Team. 2017. Active transpressional tectonics in the Andean forearc of southern Peru quantified by ^{10}Be surface exposure dating of an active fault scarp. *Tectonics*, 36, 1662-1678
53. Bierman, P.R., Gillespie, A.R., and Caffee, M.W. 1995. Cosmogenic ages for earthquake recurrence intervals and debris flow fan deposition, Owens Valley, Science, 270, 447–450.
54. Ballantyne, C.K., Stone, J.O., and Fifi eld, L.K. 1998. Cosmogenic Cl-36 dating of post-glacial landsliding at The Storr, Isle of Skye, Scotland: The Holocene, 8, 347–351
55. Sewell, R.J., Barrows, T.T., Campbell, S.D., Fifield, L.K. 2006. Exposure dating (^{10}Be, ^{26}Al) of natural terrain landslides in Hong Kong, China. Geological Society of America Special Paper 415, 131 – 146.
56. Le Roux, O., Schwartz, S., Gamond, J.F., Jongmans, D., Bourles, D., Braucher, R., Mahaney, W., Carcaillet, J., Leanni, L. 2009. CRE dating on the head scarp of a major landslide (Séchilienne, French Alps), age constraints on Holocene kinematics. *Earth and Planetary Science Letters*, 280, 236-245
57. Merchel, S., Braucher, R., Alfimov, V., Bichler, M., Bourles, D.L., Reitner, J. 2013. The potential of historic rock avalanches and man-made structures as chlorine-36 production rate calibration sites. *Quaternary Geochronology*, 18, 54-62
58. Zerathe, S., Braucher, R., Lebourg, T., Bourlès, D., Manetti, M., Leanni, L. 2013. Dating chert (diagenetic silica) using in-situ produced 10Be: possible complications revealed through the comparison with 36Cl applied on coexisting limestone. Quat. Geochronol. 17, 81–93.
59. Pánek, T. 2015. Recent progress in landslide dating: A global overview. *Progress in Physical Geography*, 39, 168–198
60. Athanassas, C.D., Bourlès, D.L., Bracucher, R., Druitt, T.H., Nomikou, P., Leanni, L. 2016. Evidence from cosmic ray exposure (CRE) dating for the existence of a pre-Minoan caldera on Santorini, Greece. *Bulletin of Volcanology*, 78: 35

61. Schwartz, S., Zerathe, S., Jongmans, D., Baillet, L., Carcailet, J., Audin, L., Dumont, T., Bourlès, D., Braucher, R., Lebrouc, V. 2017. Cosmic ray exposure dating on the large landslide of Séchilienne (Western Alps): A synthesis to constrain slope evolution. *Geomorphology*, 278, 329-344.
62. Hilger, P., Hermanns, R.L., Gosse, J.C., Jacobs, B., Etzelmüller, B., Krautblatter, M. 2018. Multiple rock-slope failures from Mannen in Romsdal Valley, western Norway, revealed from Quaternary geological mapping and ^{10}Be exposure dating. *Holocene*, 28, 1841–1854
63. Lekkas, E. and Mavroulis, S. 2016. Fault zones ruptured during the early 2014 Cephalonia Island (Ionian Sea, Western Greece) earthquakes (January 26 and February 23, Mw 6.0) based on the associated co-seismic surface ruptures. Journal of Seismology, 20, 63-78.
64. British Petroleum Company (1971) The Geological Results of Petroleum Exploration in Western Greece: Institute of Geology Subsurface Research, Athens, 10, 73.
65. Gosgrove, J.W. 2015. The association of folds and fractures and the link between folding, fracturing and fluid flow during the evolution of a fold–thrust belt: a brief review. In: Richards, F. L., Richardson, N. J., Rippington, S. J., Wilson, R.W. & Bond, C. E. (eds) Industrial Structural Geology: Principles, Techniques and Integration. Geological Society, London, Special Publications, 421,
66. Lal D., 1991. Cosmic ray labeling of erosion surfaces: in situ nuclide production rates and erosion models. *Earth Planet. Sci. Lett.* 104, 424-439.
67. Stone, J.O.H., Evans, J.M., Fifield, L.K., Allan, G.L., Cresswell B, R.G. 1998. Cosmogenic Chlorine-36 Production in Calcite by Muons. *Geochimica and Cosmochimica Acta*, 62, 433-454
68. Stone, J.O. 2000. Air pressure and cosmogenic isotope production. J Geophys Res 105, 23753–23759
69. Phillips, W.M., Hall, A.M., Mottram, R., Fifield, K.L., Sugden, D.E. 2001. Cosmogenic ^{10}Be and ^{26}Al exposure ages of tors and erratics, Cairngorm Mountains, Scotland: Timescales for the development of a classic landscape of selective linear glacial erosion. *Geomorphology*, 73-222-245
70. 70. Zerathe, S., Lebourg, T., Braucher, R., Bourlès, D. 2014. Mid-Holocene cluster of large-scale landslides revealed in the Southwestern Alps by 36Cl dating. Insight on an Alpine-scale landslide activity. *Quaternary Science Reviews*, 90, 106-127
71. Arnold, M., Merchel, S., Bourlès, D. L., Braucher, R., Benedetti, L., Finkel, R. C., Aumaître, G., Gottdang, A. and Klein M. 2010. The French accelerator mass spectrometry facility ASTER: Improved performance and developments. *Nuclear Instruments and Methods in Physics Research B*, 268, 1954– 1959.
72. Schimmelpfennig, I., Benedetti, L, Finkel, R., Pik, R., Blard, P.H., Bourlès, D., Burnard, .P, Williams A. 2009. Sources of in situ ^{36}Cl in basaltic rocks. Implications for calibration of production rates. *Quat Geochronol*. 4, 441–461
73. Braucher, R., Merchel, S., Borgomano, J., Bourlès, D.L. 2011. Production of cosmogenic radionuclides at great depth: a multi element approach. *Earth Planet Sci Lett*, 309, 1–9
74. Ying-kui, L. 2018. Determining topographic shielding from digital elevation models for cosmogenic nuclide analysis: a GIS model for discrete sample sites. *Journal of Mountain Science*, 15, 939-947
75. Cardinal, T., Audin, l., Rolland, y., Schwartz, S., Petit, C. Zerathe, S., Borgniet, L., Braucher, R., Nomade, J., Dumont, T., Guillou, V., ASTER Team. 2021. Interplay of fluvial incision and rockfalls in shaping periglacial mountain gorges. *Geomorphology*, 381: 107665
76. Cardinal, T., Rolland, Y., Petit, C., Audin, L., Zerathe, S., Schwartz, S., and the ASTER Team: Fluvial bedrock gorges as markers for Late-Quaternary tectonic and climatic forcing in the French Southwestern Alps. *Geomorphology*, 418: 108476
77. Lenart, J., Kašing, M., Pánek, T., Braucher, R., Kuda, F. 2023. Rare, slow but impressive: > 43 ka of rockslide in river canyon incising crystalline rocks of the eastern Bohemian Massif. *Landslides*, 20, 1705-1718